Solar Energy 195 (2020) 27–36

Contents lists available at ScienceDirect

Solar Energy

journal homepage: www.elsevier.com/locate/solener

Critical supercritical-boiling-number to determine the onset of heat transfer deterioration for supercritical fluids

Jinliang Xu, Haisong Zhang, Bingguo Zhu, Jian Xie*

Key Laboratory of Condition Monitoring and Control for Power Plant Equipment of Ministry of Education, North China Electric Power University, Beijing 102206, China

ARTICLE INFO

Keywords:
Supercritical fluid
Pseudo-boiling
Supercritical-boiling-number
Heat transfer deterioration
Critical heat flux
S-CO_2

ABSTRACT

Supercritical fluids such as CO_2, water and organic fluids are frequently applied in power systems. The accurate prediction of heat transfer deterioration (HTD) is important to keep the safe operation of advanced power systems such as solar driven supercritical carbon dioxide Brayton cycle. As described in textbooks, it is impossible to identify liquid from gas beyond the critical point, thus supercritical fluid is assumed to have homogeneous structure with a single-phase. The single-phase assumption cannot explain and predict supercritical heat transfer (SHT). Instead, we investigate SHT by the pseudo-boiling concept. Heat transfer is analogized between supercritical pressure and subcritical pressure to create a new non-dimensional supercritical-boiling-number *SBO*, representing the bubble expansion induced momentum force against the inertia force when it is coupled with the ratio of liquid density with respect to vapor density. Our study reveals sudden changes from normal heat transfer (NHT) to heat transfer deterioration (HTD) with obvious temperature peak when crossing a critical *SBO*, which is 5.126×10^{-4}, 2.018×10^{-4}, 1.653×10^{-4} and 1.358×10^{-4} for CO_2, H_2O, R134a and R22, determined by a large quantity of database. Our work paves a new way to understand the SHT mechanism and supports the heterogeneous structure of liquid-like fluid and vapor-like fluid for supercritical fluids.

1. Introduction

Supercritical fluids were discovered by experimentally identifying the discontinuities of the sound in a cannon barrel filled with different fluids (Baron Charles Cagniard de la Tour 1822). Since then, the research and development of supercritical fluids have been an exciting field (Berche et al., 2009). Recently, supercritical fluids have been recommended for various applications in food preparation, pharmaceutical product, functional material, micro/nano system, bio-fuel (Bolmatov et al., 2013; Kiran et al., 2000; McHardy and Sawan, 1998). Supercritical fluid is attractive to be applied in advanced power generation system to have high cycle efficiency and small system size (Cheang et al., 2015; Stein and Buck, 2017). In such a system, a heater couples the heat source with ultra-high heat flux and the supercritical pressure cycle (Xu et al., 2018; Sun et al., 2018). The heat source can be nuclear energy, solar energy, or fossil energy. The accurate evaluation of supercritical heat transfer is crucial to design a power generation system (Pizzarelli, 2018). Considering a solar driven S-CO_2 power cycle, if the solar receiver is not well cooled by the supercritical CO_2 fluid, the solar receiver will be burned out. This phenomenon should be avoided in the design stage.

As defined in textbooks, the fluid phase diagram consists of a subcritical pressure region having liquid phase and gas phase, and a supercritical pressure region with a single-phase structure (Cengel and Boles, 2006). At subcritical pressure, the *latent heat of evaporation* (i_{fg}) quantifies how much heat is needed to convert liquid to vapor per unit mass at a constant saturation temperature. The value of i_{fg} is decreased with increase of pressures, and becomes zero at the critical point *c* (see Fig. 1(a)). At supercritical pressure, the pseudo-critical point *pc* is defined at the maximum specific heat. Heat cannot be added to supercritical fluid at a constant temperature but should accompany a temperature rise. Near the *pc* region, the thermo-physical properties are changed significantly to cause the buoyancy effect and acceleration effect (Negoescu et al., 2017; Kurganov et al., 2012). The single-phase supercritical fluid concept and the two effects explained and predicted the supercritical heat transfer for more than half century. The developed heat transfer correlations are different among different research groups, and usually they are only suitable for their own data ranges (Huang et al., 2016). Most importantly, under specific condition such as high heat flux q_w and low mass flux *G*, an abrupt wall temperature peak (called heat transfer deterioration HTD) occurs (see Fig. 1(b) with the data from Wang et al. (2011)). The HTD may cause the heater burnout, thus it should be avoided for practical operation. There is no reliable theory to explain and predict the onset of HTD currently.

* Corresponding author.
E-mail address: xiejian90@ncepu.edu.cn (J. Xie).

https://doi.org/10.1016/j.solener.2019.11.036
Received 5 August 2019; Received in revised form 18 September 2019; Accepted 12 November 2019

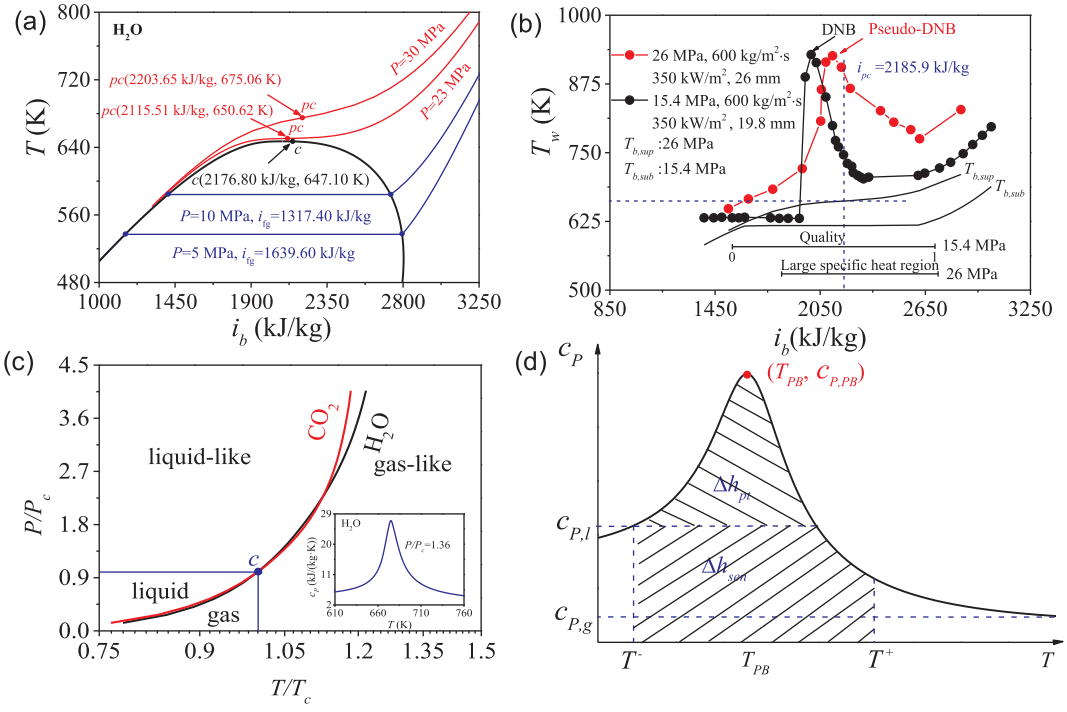

Fig. 1. Thermodynamics and heat transfer behavior at subcritical and supercritical pressures. (a) temperature (T)-enthalpy(i) curves at different pressure levels to show isothermal two-phase regime at subcritical pressure and temperature rise at supercritical pressure. (b) significant temperature overshoot observed for heat transfer for subcritical 15.4 MPa water and supercritical 26 MPa water with the data cited from Wang et al (2011), in which DNB means the departure from nucleating boiling. (c) the P/P_c-T/T_c curves characterize the transition from liquid to vapor at subcritical pressures and from liquid-like to gas-like at supercritical pressures. (d) the c_p curve near the Widom line coincided with the pseudo-critical point pc, showing that the added energy can be divided into two parts, one part for temperature rise, and the other part to overcome the molecular attraction.

The single-phase supercritical fluid concept is questioned by physicists in recent years. Simeoni et al. (2010) used the X-rays scattering and molecular dynamics simulation to decide the velocity of acoustic waves in nanoscale for supercritical argon. They observed that the supercritical fluid actually includes a gas-like fluid region and a liquid-like fluid region when crossing the Widom line. Gorelli et al. (2013) observed the abrupt variations in the dynamical properties versus pressure and temperature (T/T_c = 2–5 and P/P_c = 510–10^3), where T_c is the critical temperature and P_c is the critical pressure. In the Terahertz frequency region, the sound propagation shows a sudden transition when crossing the gas-like fluid regime and the liquid-like fluid regime, involving the coupling between acoustic waves and thermal waves. Thus, a dynamic line can be determined in the phase diagram. Gallo et al. (2014) studied the thermodynamic properties of supercritical water by analyzing the experimental data and numerical results. They found that when approaching the critical point, the curves linking the maxima of the response functions shrink to a single line (Widom line), which identifies a clear transition from a liquid-like phase to a gas-like phase. The two regimes of liquid-like and gas-like are shown in Fig. 1(c) for supercritical CO_2 and H_2O. The Widom line beyond the critical point is determined in terms of the maximum specific heat calculated by the NIST software, matching the prediction of P/P_c = exp [5.55(T/T_c-1)] suggested by Banuti (2015).

Except the sharp wall temperature peak observed for supercritical fluids, other experimental evidences are also reported for supercritical heat transfer to support the pseudo-boiling assumption involving the two phases of vapor and liquid. Holman et al. (1965) experimentally studied the forced convective heat transfer of Freon 12 in a vertical annulus, indicating the pseudo-boiling phenomenon near the critical temperature. Their visualization photos gave a vapor film boiling type of the process. Stewart et al. (1973) studied the supercritical heat transfer with water flowing in horizontal tubes at uniform heat flux. The measured oscillation frequencies are shown to be related to the pressure oscillations induced by a standing pressure wave between the test section entry and exit. The varied heat transfer coefficients are associated with the local pressure fluctuations. In other words, the oscillation characteristic of the subcritical boiling also appears at supercritical pressures. Unfortunately, the pseudo-boiling concept has never been incorporated into the theoretical/numerical treatment of supercritical heat transfer.

The present paper aims at the development of new criteria to predict the occurrence of heat transfer deterioration (HTD) for various supercritical fluids. Compared with other works in the literature, the single-phase fluid assumption of supercritical fluids is not used. Instead, we apply the pseudo-boiling concept. Holding this concept, we made a connection of supercritical heat transfer and subcritical heat transfer, yielding a new supercritical-boiling-number *SBO*. We found that HTD is well controlled by *SBO*. The critical *SBO* values are determined for four widely used fluids of CO_2, H_2O, R134a and R22 to judge the occurrence of HTD.

2. Heat transfer analogy between subcritical and supercritical pressures

In this paper, we abandon the single-phase assumption, but use the pseudo-boiling concept to handle the supercritical heat transfer. The studied problem is defined as a convective heat transfer in a vertical upflow tube at supercritical pressure. The fluid receives a uniform heat flux from inner tube wall. Because the two flow sections beyond the main heating section are sufficiently long, the flow is well developed in the main heating section. The pseudo-boiling of supercritical heat transfer can be explained using the c_p curve near the pc region, where c_p is the specific heat (see Fig. 1(d)). The change from liquid-like fluid to vapor-like fluid takes place at the Widom line, coincided with the pseudo-critical temperature T_{pc} (Banuti, 2015). The "boiling" of supercritical fluid starts at a temperature T^-, that is smaller than T_{pc}, and

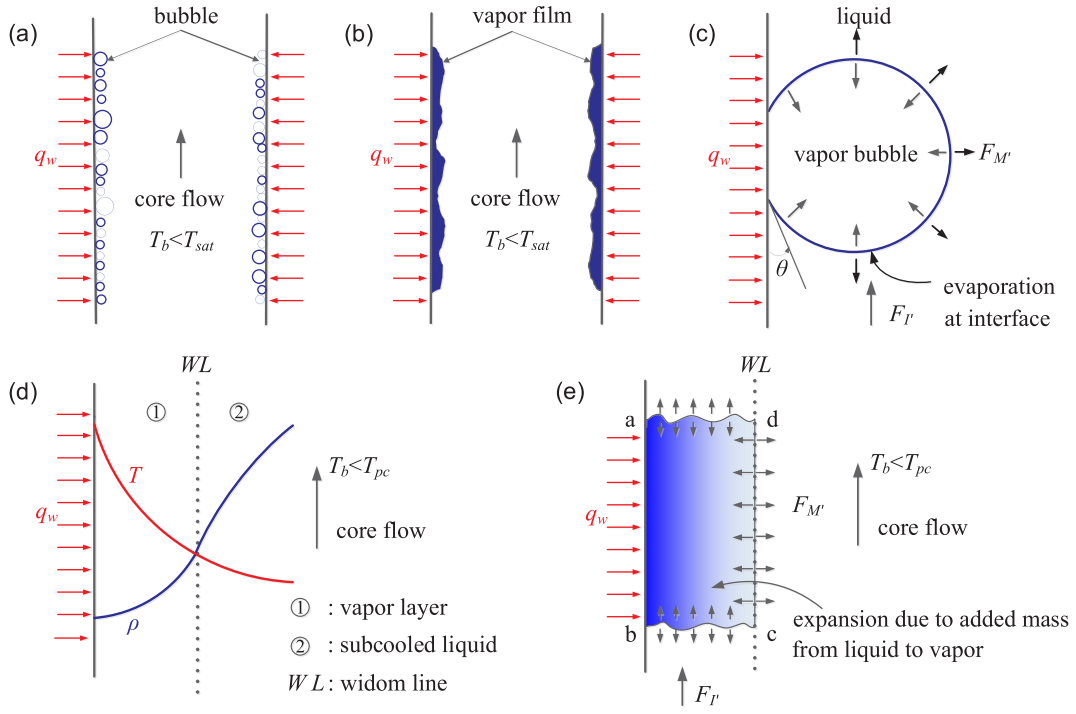

Fig. 2. The similarity between subcooled boiling at subcritical pressure and supercritical heat transfer in vertical tubes. (a) subcooled boiling at subcritical pressure having bubbles on the all and no net vapor generation in the core flow. (b) the vapor blanket on the wall which may trigger the heat transfer deterioration. (c) forces applied on the bubble interface, where θ is the bubble contact angle on the wall, $F_{M'}$ and $F_{I'}$ are the bubble expansion induced momentum force and inertia force respectively. (d) the Widom line characterizes the vapor-like fluid near the wall and the liquid-like fluid beyond the Widom line at supercritical pressure; (e) the forces applied on the vapor layer at supercritical pressure.

ends at a temperature T^+, that is larger than T_{pc}. Then, the required energy per unit mass for the boiling from liquid-like to vapor-like is

$$\Delta i = \int_{T^-}^{T^+} c_P(T)\mathrm{d}T = i(T^+) - i(T^-) = \Delta i_{sen} + \Delta i_{ma} \tag{1}$$

The added energy can be divided into two parts. The first part, represented by the shaded Δi_{sen} area, contributes the temperature rise from T^- to T^+. The second part, represented by the shaded Δi_{ma} area, overcomes the molecular attraction to reach a sparse distribution from a dense distribution of the fluid particles. This statement is different from boiling at subcritical pressures during which the temperature remains constant and all the energy is consumed to overcome the molecular attraction. The determination of T^- and T^+ can be found in Banuti (2015).

The supercritical heat transfer is analogized to the subcooled boiling at subcritical pressures. For subcritical boiling, bubbles nucleate and grow on the wall. These bubbles detach the wall to merge with and are condensed by the subcooled liquid of the core flow. Thus, vapor is not accumulated in the tube core (see Fig. 2(a)). On the contrary, bubbles do not depart the wall and coalesce to create a vapor blanket (see Fig. 2(b)), leading to a sharp wall temperature peak (HTD). The formation of vapor blanket is associated with an important parameter, K_1 number (Kandlikar, 2004). For a wall attached bubble, the evaporation on vapor-liquid interface generates an evaporation mass flux q_w/i_{fg}, yielding a force on the bubble interface (see Fig. 2(c))

$$F_{M'} = \left(\frac{q_w}{i_{fg}}\right)^2 \frac{D}{\rho_g} \tag{2}$$

where D and ρ_g are bubble diameter and vapor density, respectively. On the other hand, the inertia force applied on the bubble is

$$F_{I'} = \frac{G^2 D}{\rho_f} \tag{3}$$

where ρ_f is the liquid density. K_1 number reflects the evaporation momentum force competed with the inertia force:

$$K_1 = \frac{F_{M'}}{F_{I'}} = \left(\frac{q_w}{G i_{fg}}\right)^2 \frac{\rho_f}{\rho_g} = \frac{\rho_f}{\rho_g} Bo^2 \tag{4}$$

where Bo is the boiling number: $Bo = q_w/(Gi_{fg})$. For a specific density ratio with a given working fluid, the boiling number is of significance in identifying the heat transfer mechanism. An earlier work by Xu et al. (2005) reveals that depending on Bo, microscale boiling heat transfer can be clarified into a nucleate boiling regime, a liquid film convective heat transfer regime and a mixed heat transfer regime.

Now, we deal with the supercritical heat transfer using the pseudo-boiling concept (see Fig. 2(d)–(e)). A thin vapor layer behaves $T_w > T_{pc} > T_b$, where T_w is the temperature at the inner wall, T_b is mainstream fluid temperature. Beyond the Widom line (also T_{pc}) is the core flow with high fluid density, which is regarded as the "subcooled" liquid because $T_b < T_{pc}$. The Widom line reaches a "saturation temperature". The mass transfer due to the evaporation on the Widom line results in an increment of vapor mass to expand the vapor layer thickness. During this process, the evaporation on the Widom line is resulted from the saturation liquid heated by the superheating vapor. There is a momentum force due to vapor expansion on the Widom line (T_{pc} location). If the inertia force is sufficient strong to overcome the momentum force, the vapor layer thickness is decreased to keep normal heat transfer (NHT) without apparent wall temperature peak. On the contrary, the vapor layer grows significantly resulting in heat transfer deterioration (HTD) to have apparent peak of wall temperature, which is analogy to the subcooled boiling at subcritical pressure.

For boiling at subcritical pressure, q_w/i_{fg} means the evaporation mass flux on the vapor-liquid interface. For supercritical heat transfer, Δi in Eq. (1) quantifies the phase change enthalpy from liquid-like fluid to vapor-like fluid. Because the "latent heat of evaporation" does not exist at supercritical pressure, the evaporation mass flux across the

Widom line is scaled as $q_w/\Delta i$. Eq. (1) indicates that Δi is dependent on T^- and T^+. Because the determination of T^- and T^+ is difficult, a coefficient k is introduced to relate the phase change enthalpy Δi with i_{pc} (enthalpy at pseudo-critical point), which is a physical property of supercritical fluid (see the example values in Fig. 1(a) for water at the pc state):

$$\Delta i = i(T^+) - i(T^-) = k \cdot i_{pc} \tag{5}$$

Then, the mass increment of the vapor-like fluid is scaled as q_w/i_{pc} for supercritical boiling. The supercritical-boiling-number is expressed as

$$SBO = \frac{q_w}{G i_{pc}} \tag{6}$$

Later we will show that, indeed, *SBO* controls the transition from NHT to HTD.

3. Experiment setup and test section

The supercritical-boiling-number *SBO* is verified by an expanded database with supercritical carbon dioxide, water, R134a and R22, respectively. We find that *SBO* plays an important role in distinguishing the transition from NHT to HTD. Attention has been focused on the supercritical CO_2 Brayton cycle for power generation, in which a heater is used to extract high heat flux. Based on the cycle requirement (Xu et al., 2018; Sun et al., 2018), the operation pressure should be > 20 MPa with heat flux more than 100 kW/m^2. The available experimental data in references covered narrow pressure range of ~8 MPa, which is not sufficient to evaluate the effectiveness of the supercritical-boiling-number. Thus, we provided additional experiment data, covering the ranges of 7.5–21.1 MPa for pressures P, 488–1600 kg/m^2 s for mass fluxes G and 74–413 kW/m^2 for inner heat fluxes q_w. Totally 79 runs of experimental data are obtained.

Our S-CO_2 heat transfer experimental setup consists of a gas-vacuum/CO_2-charging system, a convective CO_2 loop, a cooling water loop, an electric heating system (see Fig. 3). Initially, non-condensable gas in the closed system was vacuumed to environment. Then, the 99.99% purity CO_2 was charged into the system. During operation, the CO_2 flow rate in the loop system was driven by a piston pump. Either one of the two flow-rate-meters measured the CO_2 flow rate, which then flowed through the tube side of a recuperator heat exchanger, a preheater and a test tube. The CO_2 vapor at the test tube outlet entered the shell side of the recuperator heat exchanger and then was cooled by a cooling water loop. Low direct-current (DC) voltage was directly applied on the test tube. Changing the DC voltage easily altered the heating power. The major parts of the loop were wrapped by thick thermal insulation material to decrease the heat loss to environment.

The test tube material is 1Cr18Ni9Ti (see Fig. 4). The tube was vertically positioned having up-flow direction. Two test tubes were used, both having the total length of 3600 mm, effective heating length of 2000 mm and wall thickness of 2.0 mm. One tube had an inner diameter of 8.0 mm ($d_{in} = 8.0$ mm), the other had an inner diameter of 10.0 mm ($d_{in} = 10.0$ mm). A capacitance impact welding machine welds thermocouple wires on the outer tube surface. There are 39 cross-sections along the flow direction, a couple of thermocouples are welded on each cross-section. In such a way, the continuous wall temperatures are detected. The test tube is thermally insulated to prevent heat leakage to environment. The mass flux G is defined as

$$G = m/\left(\frac{1}{4}\pi d_{in}^2\right) \tag{7}$$

where m and d_{in} are mass flow rate and inner diameter of the test tube ($d_{\mathrm{in}} = 10.0$ mm or 8.0 mm here), respectively. The inner wall heat flux is defined as

$$q_w = \frac{Q}{\pi d_{in} L} = \frac{m(i_{out} - i_{in})}{\pi d_{in} L} \tag{8}$$

where the heating length is $L = 2000$ mm in this study, i_{out} and i_{in} are outlet CO_2 enthalpy and inlet CO_2 enthalpy at operation pressure. Because we need to plot the curves of $T_w \sim i_b$, where i_b is the axial length dependent enthalpy of the CO_2 fluid, which is decided in terms of the energy conservation equation:

$$i_b = i_{b,in} + \frac{q_w \pi d_{in} z}{m} \tag{9}$$

where $i_{\mathrm{b,in}}$ is the enthalpy characterized by pressure P and inlet CO_2 temperature T_{in}, the flow length z starts from the heating location. According to the one-dimensional thermal conduction principle with internal heat source, the inner wall temperature T_w is computed in terms of $T_{w,out}$ (outer wall temperature measurement) and q_w:

$$T_w = T_{w,out} - \frac{q_w r_{in}}{2\lambda}\left(\frac{a^2 - 2\ln a - 1}{1 - a^2}\right) \tag{10}$$

where $a = r_{in}/r_{out}$ (r_{in} is the inner tube radius and r_{out} is the outer tube radius).

A DMF-1-3-B Coriolis mass-flow-meter with a range of 0–1000 kg/h, or a DMF-1-2-A mass-flow-meter with a range of 0–200 kg/h, measured the mass flow rate m, both having an uncertainty of 0.2%. A Rosemount 3051 pressure transducer measured the CO_2 pressure at the test tube inlet with an uncertainty of 0.1%. Two jacket thermocouples measured fluid temperatures at the test tube inlet T_{in} and outlet T_{out}, having an uncertainty of 0.5 °C after calibration. Wall temperature measurements involved an uncertainty of 0.2 °C. A data acquisition system ADAM-4118/4117 collected all the data samples during system operation. The error transmission principle is helpful to evaluate the errors of various parameters, yielding the uncertainties of 5.6% for q_w and 8.46% for heat transfer coefficient.

4. Results and discussion

4.1. Normal heat transfer and heat transfer deterioration

Our experiment and other experiments in literature support the developed supercritical-boiling-number. When S-CO_2 flows in vertical tubes under uniform heating boundary condition, the transition from normal heat transfer to heat transfer deterioration takes place at 5.126×10^{-4}. A pair of running cases are shown in Fig. 5 with $d_{in} = 10.0$ mm. Fig. 5(a) shows normal heat transfer without temperature overshoot at $P = 21.011$ MPa, which is ~3 times of the critical pressure 7.377 MPa. Fig. 5(b) shows heat transfer deterioration with obvious wall temperature peak of 34.3 K. We note that Fig. 5(a) and (b) share similar inner heat flux q_w and mass flux G. The high-pressure-operation keeps *SBO* to be smaller than the critical value 5.126×10^{-4}, maintaining normal heat transfer (see Fig. 5(a)). The near critical pressure operation yields the *SBO* just beyond the critical value 5.126×10^{-4} to yield heat transfer deterioration (see Fig. 5(b)). Wall temperature overshoot ΔT is an important indicator to judge if heat transfer deterioration occurs, which should be determined for each experiment case. In the present study, ΔT is determined based on wall temperature curve along flow length, or versus bulk fluid enthalpies (see Fig. 5b). Wall temperature curve according to normal heat transfer route is expressed as a dashed line. ΔT is the peak value of the practical wall temperature subtracting the value according to normal heat transfer route. For heat transfer deterioration, ΔT can be large in the range from several degrees to more than 100 °C, while it does not appear or is less than several degrees for normal heat transfer.

In the literature, the occurrence of HTD is correlated in the form of q_w/G (Shiralkar & Griffith, 1969; Kim et al., 2005; Zhang et al., 2018). Such treatment is suitable for identical pressure operation, but is not correct for different pressures. Fig. 6 shows S-CO_2 heat transfer in

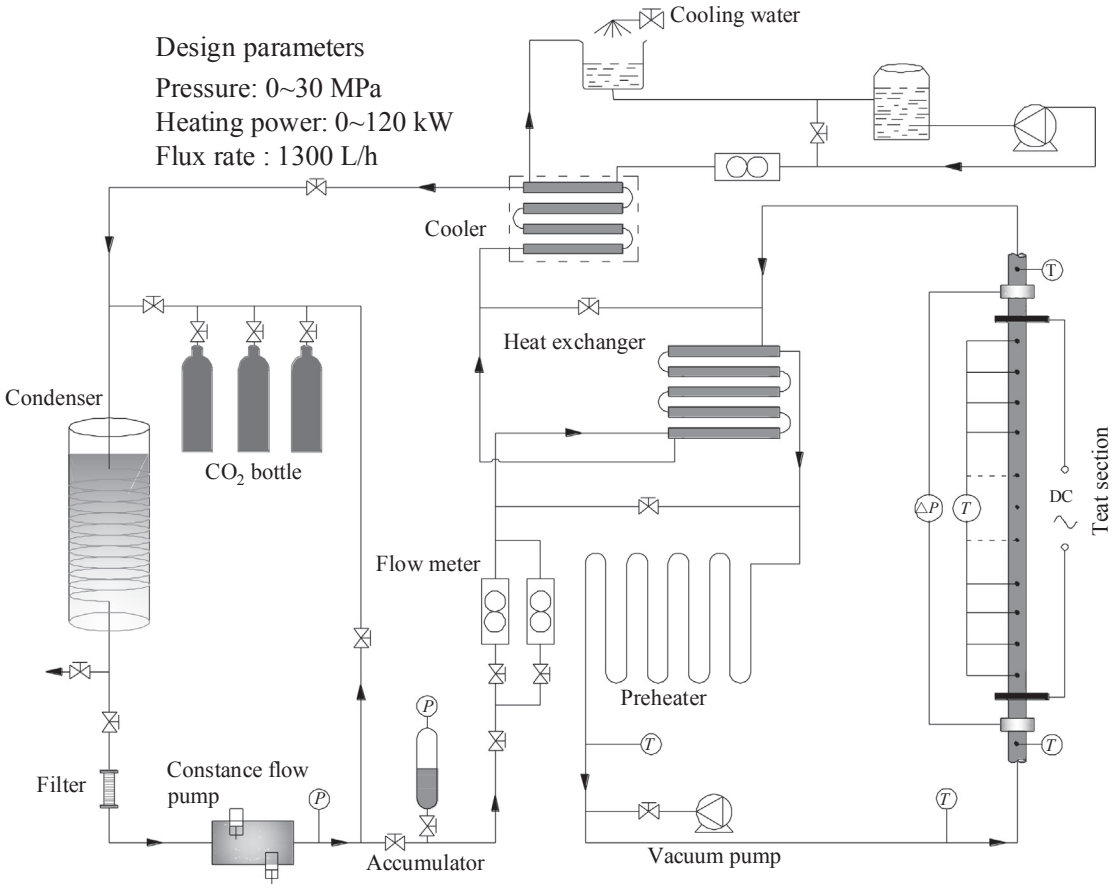

Fig. 3. Experimental setup of the present study.

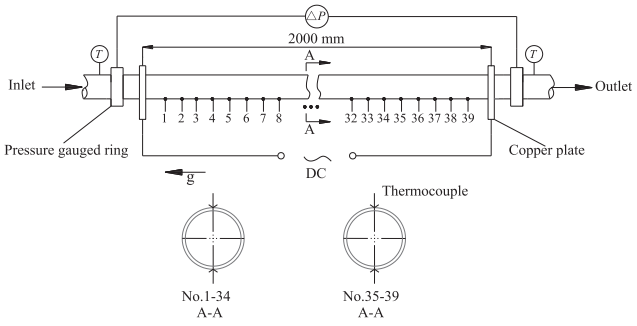

Fig. 4. The test tube (inner tube diameters of 8.0 mm and 10.0 mm).

d_{in} = 8.0 mm tube. At similar pressure ~8 MPa, the increase of q_w/G from 0.1256 kJ/kg to 0.175 kJ/kg results in the transition from normal heat transfer shown in Fig. 6(a) to heat transfer deterioration shown in Fig. 6(b). This is because *SBO* in Fig. 6(b) just exceeds the critical value. We keep nearly identical q_w/G in Fig. 6(b)–(d). The increase of pressures to 15.435 MPa and 20.822 MPa decreases *SBO* to be smaller than the critical value, switching heat transfer deterioration back to normal heat transfer (see Fig. 6(c)–(d)). In summary, Figs. 5 and 6 indicate that heat transfer deterioration is controlled by *SBO*, not by q_w/G.

To further identify the sudden change between normal heat transfer and heat transfer deterioration when crossing the critical *SBO*, heat transfer data of organic fluids are cited from references to support this conclusion. Fig. 7(a) and (b) show the R134a data. Smooth wall temperature rise along flow length is shown in Fig. 7(a) to behave normal heat transfer due to *SBO* below the critical value 1.653×10^{-4}. Alternatively, the sharp wall temperature peak occurs in Fig. 7(b) due to *SBO* exceeds the critical value 1.653×10^{-4}. Similar phenomenon also appears in Fig. 7(c) and (d). The only difference is that different working fluids have different critical *SBO* to govern the onset of heat transfer deterioration.

4.2. Transition criteria for four working fluids

The inner wall temperatures T_w are plotted versus bulk fluid enthalpies, in which Fig. 8(a) shows normal heat transfer with T_w gradually increases with increases of i_b without apparent wall temperature overshoot, and Fig. 8(b) shows HTD with a significant wall temperature overshoot ΔT = 128 °C, where ΔT is defined as the maximum wall temperature subtracting the temperature according to a normal heat transfer route *ab*. Our measurement data and other data in the literature are used to create a map of the wall temperature overshoot against the supercritical boiling number in Fig. 8(c), including 79 data points of our own data, 2 data points with d_{in} = 2 mm from Li et al. (2010), 3 data points with d_{in} = 4.5 mm from Kim and Kim (2011), 6 data points with d_{in} = 6.32 mm from Bae et al. (2010), 7 data points with d_{in} = 8 mm from Jiang (2015) and 4 data points with d_{in} = 10 mm from Liu et al. (2017). Fig. 8(c) clearly shows the sudden change of the two heat transfer modes, which is controlled by *SBO*. The critical *SBO* is determined as 5.126×10^{-4}. This value is suitable not only for our own experiment data, but also for other data in the literature (Li et al., 2010; Kim and Kim, 2011; Bae et al., 2010; Jiang, 2015; Liu et al., 2017).

To examine the generalness of the supercritical-boiling-number, the supercritical heat transfer data is tested with other fluids. Water is widely used in heat exchangers for various thermodynamic cycles to convert heat into power (coal-fired, nuclear energy or solar energy driven power plants). Due to the importance in keeping the safety

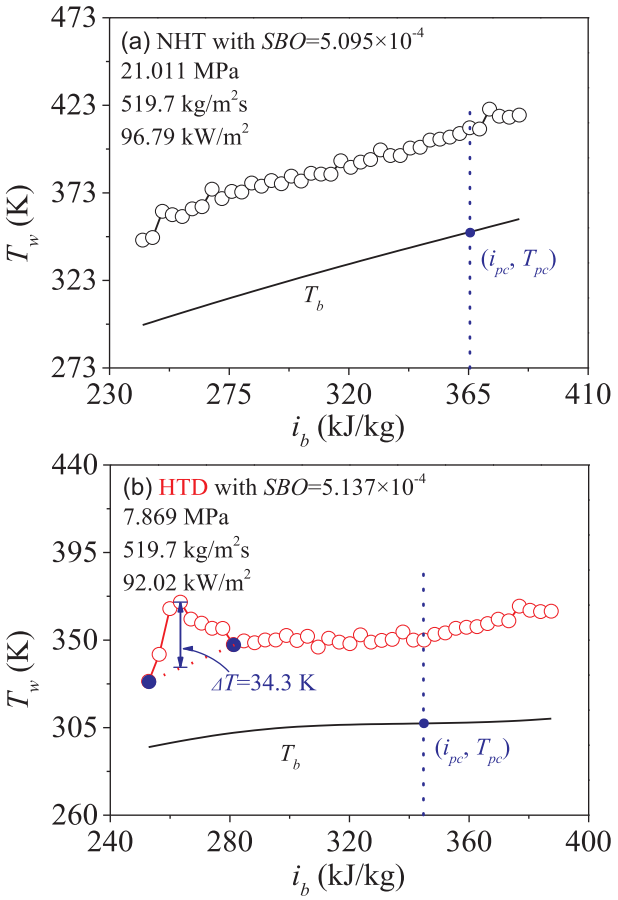

Fig. 5. Sudden changes of two heat transfer characteristics with small deviation from the critical *SBO* (our data for S-CO_2 heat transfer, d_{in} = 10.0 mm, i_{pc} = 365.53 kJ/kg, T_{pc} = 350.65 K in (a); i_{pc} = 344.75 kJ/kg, T_{pc} = 307.15 K in (b)).

operation of nuclear power plants, a large quantity of experimental data has been acquired from 1950s, but the mechanism of HTD is an open question until now. Fig. 8(d) shows a NHT case without apparent wall temperature overshoot for supercritical water at P = 28 MPa, G = 1536 kg/m^2 s, q_w = 250 kW/m^2 in a 17 mm diameter tube. On the other hand, a HTD case generates a wall temperature overshoot of 217 K at P = 23 MPa, G = 600 kg/m^2 s, q_w = 300 kW/m^2 in a 26 mm diameter tube (see Fig. 8). Surprisingly, *SBO* also controls the transition from NHT to HTD, having a critical value of 2.018 × 10^{-4} (see Fig. 8(f)).

As demanded by the development of advanced refrigeration systems or organic Rankine cycles using organic fluids with low boiling temperatures, experimental data are cited from the literature to evaluate the usefulness of *SBO*. The regime maps are plotted in Fig. 9(a) for supercritical R134a and Fig. 9(b) for supercritical R22. Sudden changes of the two heat transfer regimes are found when crossing the critical supercritical boiling number, which is 1.653 × 10^{-4} for R134a and 1.358 × 10^{-4} for R22. The only difference is the different critical *SBO* for different working fluids. We note that R134a and R22 may be replaced by other new fluids such as R422D having low environment impact (Aprea and Maiorino, 2011), but it does not influence the evaluation of *SBO* on the supercritical heat transfer. There are not sufficient experiment data for new fluids regarding this purpose, which is the reason to use the data of R134a and R22 here.

Fig. 9(c) summarizes the results, containing 359 data points to create such a regime map for the four fluids. The four fluids are randomly selected and independent with each other, having significantly different critical parameters (see Table 1). For example, the critical pressure of 22.06 MPa for water is three times of 7.377 MPa for CO_2, thus we conclude the general guideline of supercritical-boiling-number to define the supercritical heat transfer in vertical up-flow tubes. For subcritical boiling, critical heat flux (CHF) is defined as a heat flux to trigger obvious wall temperature overshoot. The term of CHF is still used for supercritical heat transfer, which is defined at the onset of heat transfer deterioration:

$$q_{w,CHF} = SBO_{CHF} \cdot G \cdot i_{pc} \tag{11}$$

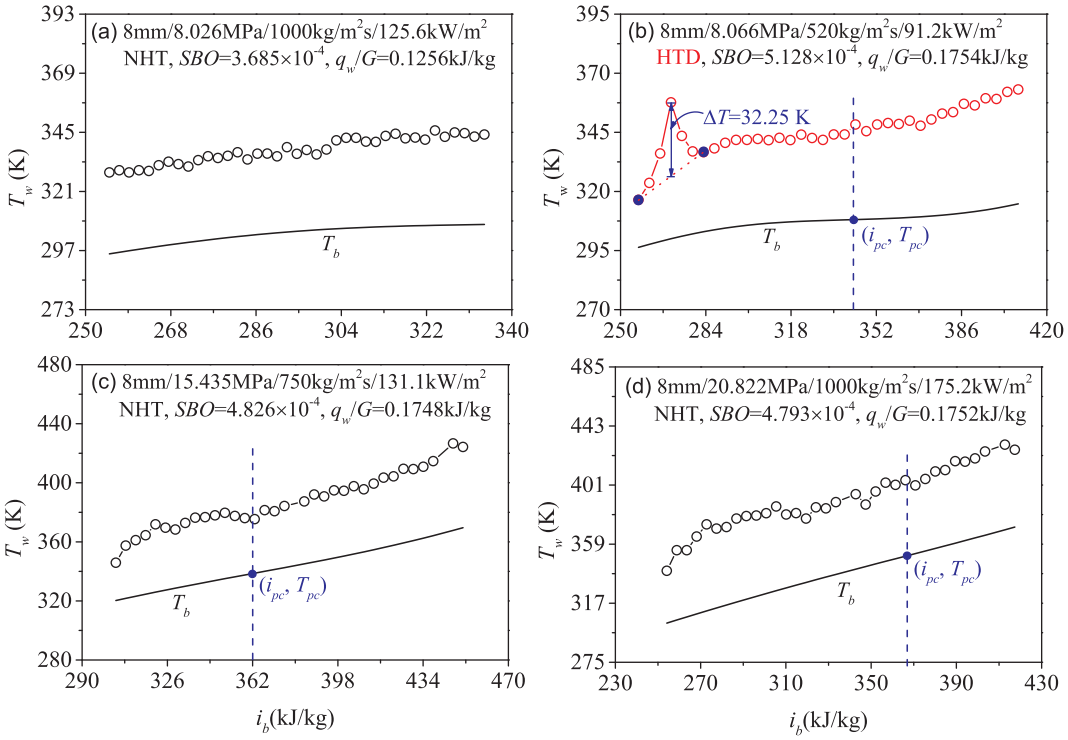

Fig. 6. Experiment results showing that HTD depends on *SBO*, not depending on q_w/G.

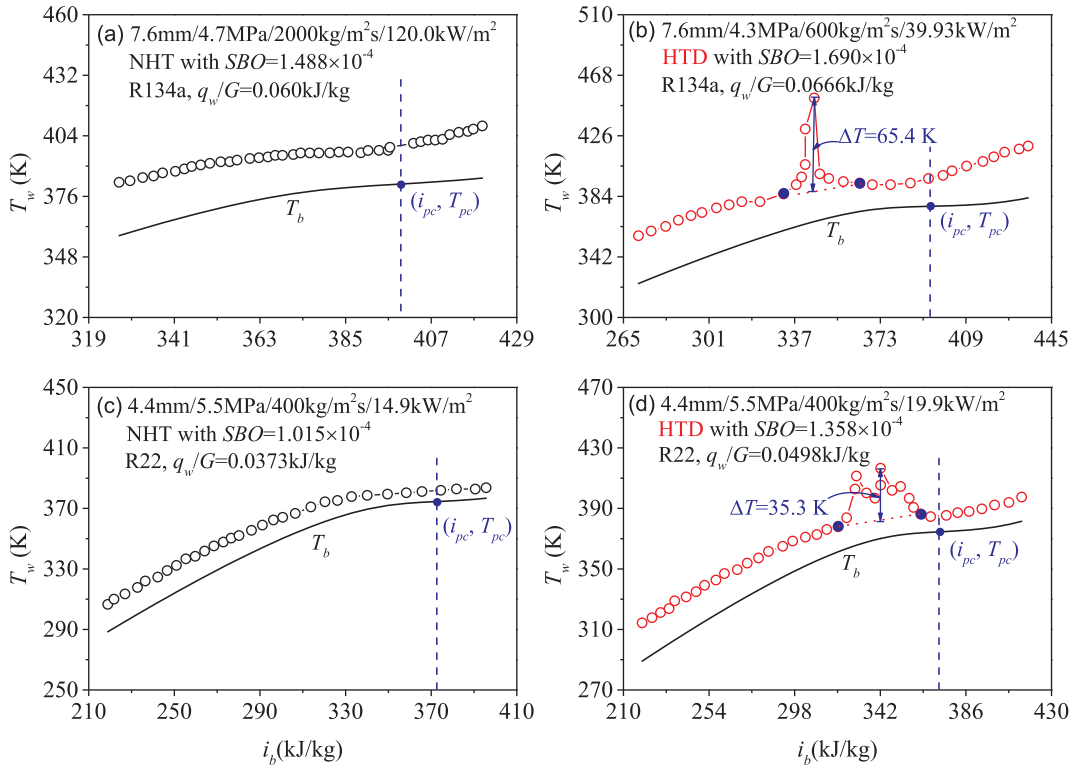

Fig. 7. Sudden changes between normal heat transfer and heat transfer deterioration when crossing the critical supercritical boiling number *SBO* for R134a and R22 ((a) for R134a data from Zhang (2015), (b) for R134a data from Kang and Chang (2009), (c) and (d) for R22 data from Yamashita et al (2003)).

In fact, SBO_{CHF} is the critical supercritical-boiling-number, which is 5.126×10^{-4} for CO_2, 2.018×10^{-4} for H_2O, 1.653×10^{-4} for R134a and 1.358×10^{-4} for R22, respectively. At a given working fluid, the critical heat flux is linearly correlated as G and i_{pc}. Eq. (11) is newly called the linear law of the supercritical heat transfer. The wall temperature overshoot ΔT is illustrated against $q_w/q_{w,CHF}$ in Fig. 9(d). There is no temperature overshoot when $q_w/q_{w,CHF} < 1$ to ensure the safety operation of the system. On the contrary, the wall temperature overshoot is significant when $q_w/q_{w,CHF} > 1$, which should be avoided for practical operation of the system.

We note that heat flux is the added heating power divided by surface area. Thus, it is not dependent on wall conditions and fluid properties for both boiling at subcritical pressure and supercritical heat transfer. However, the critical heat transfer characterizing the heat flux at the onset of heat transfer deterioration depends on wall conditions and fluid properties, see Eq. (11). The present paper deals with smooth tube. The enhanced heat transfer tube using internal geometry structure definitely enhances heat transfer to increase critical heat transfer, which is beyond the scope of this paper.

4.3. Comments on supercritical-boiling-number

SBO helps us to identify the influence of multi-parameters on heat transfer. The studied problem is defined by heat flux, mass flux, operation pressure and inner tube diameter. The heat transfer behavior is not dependent on any one of these parameters alone, but dependent on *SBO*, in which q_w/i_{pc} scales the mass transfer from liquid-like fluid to vapor-like fluid, while G quantifies the effect of inertia force. A smaller q_w/i_{pc} and/or larger G maintains smaller *SBO* to keep normal heat transfer. The effect of supercritical pressure is implicitly reflected by enthalpy at the pseudo-critical point, i_{pc}. The values of i_{pc} are increased with increase of pressures. Thus, a same added energy results in smaller mass transfer from liquid-like fluid to vapor-like fluid to suppress vapor layer growth at higher operation pressure, improving heat transfer. In our CO_2 heat transfer experiment, three pressure levels are tested with ~8 MPa level, ~16 MPa level and ~22 MPa level. It is observed that when heat flux and mass flux are the same, a heat transfer deterioration case at a lower pressure level of ~8 MPa would be switched to a normal heat transfer case when operating at a higher-pressure level of ~16 MPa or ~22 MPa (see Figs. 5 and 6). *SBO* rightly interprets the influence of pressures on supercritical heat transfer. The inner tube diameters d_{in} has complicated influence on heat transfer and there is no general conclusion on that (Mayinger and Scheldt, 1984; Ackerman, 1970). The regime maps of heat transfer behavior involve the database with different inner tube diameters, in which the data of d_{in} = 2 mm, 4.5 mm, 6.32 mm, 8 mm and 10 mm are used in Fig. 8(c) for CO_2, the data of d_{in} = 7.6 mm, 10 mm, 16 mm, 17 mm, 18.5–19.8 mm, 24.4 mm, 26 mm and 38 mm are used for water (Wang et al., 2011; Ackerman, 1970; Zhao et al., 2014; Li, 2011; Wang, 2012; Zhang et al., 2012; Wang et al., 2013; Hu et al., 2001; Pan et al., 2011; Shen et al., 2014; Shen et al., 2016; Lei et al., 2017; Zhu et al., 2009; Hu, 2001; Mokry et al., 2011), the data of d_{in} = 7.6 mm, 9.4 mm, 10 mm and 25 mm are used for R134a (Zhang, 2015; Cui and Wang, 2018a; Cui and Wang, 2018b; Kang and Chang, 2009; Chen et al., 2016), and the data of d_{in} = 4.4 mm, 6 mm, 9 mm, 10 mm,13 mm and 13.5 mm are used for R22 (Yamashita et al., 2003; Dubey et al., 2018). Because the d_{in} ranges from 2 mm to 38 mm are covered for the four fluids to create the heat transfer regimes, the tube diameters do not influence the crossover between NHT and HTD. However, the tube diameters affect the amplitude of wall temperature overshoot and the minimum heat transfer coefficients when HTD occurs, which is beyond the scope of this paper. As noted previously, the treatment using the single-phase fluid concept together with the variations of physical properties cannot explain and predict the correct trend of supercritical heat transfer (Huang et al., 2016), but the problem can be successfully treated using the pseudo-boiling concept with the solid assumption of heterogeneous structure of liquid-like fluid and vapor-like fluid. The data of NHT and HTD can be seen in Tabs. S1-S4 for the four working fluids in supplementary material.

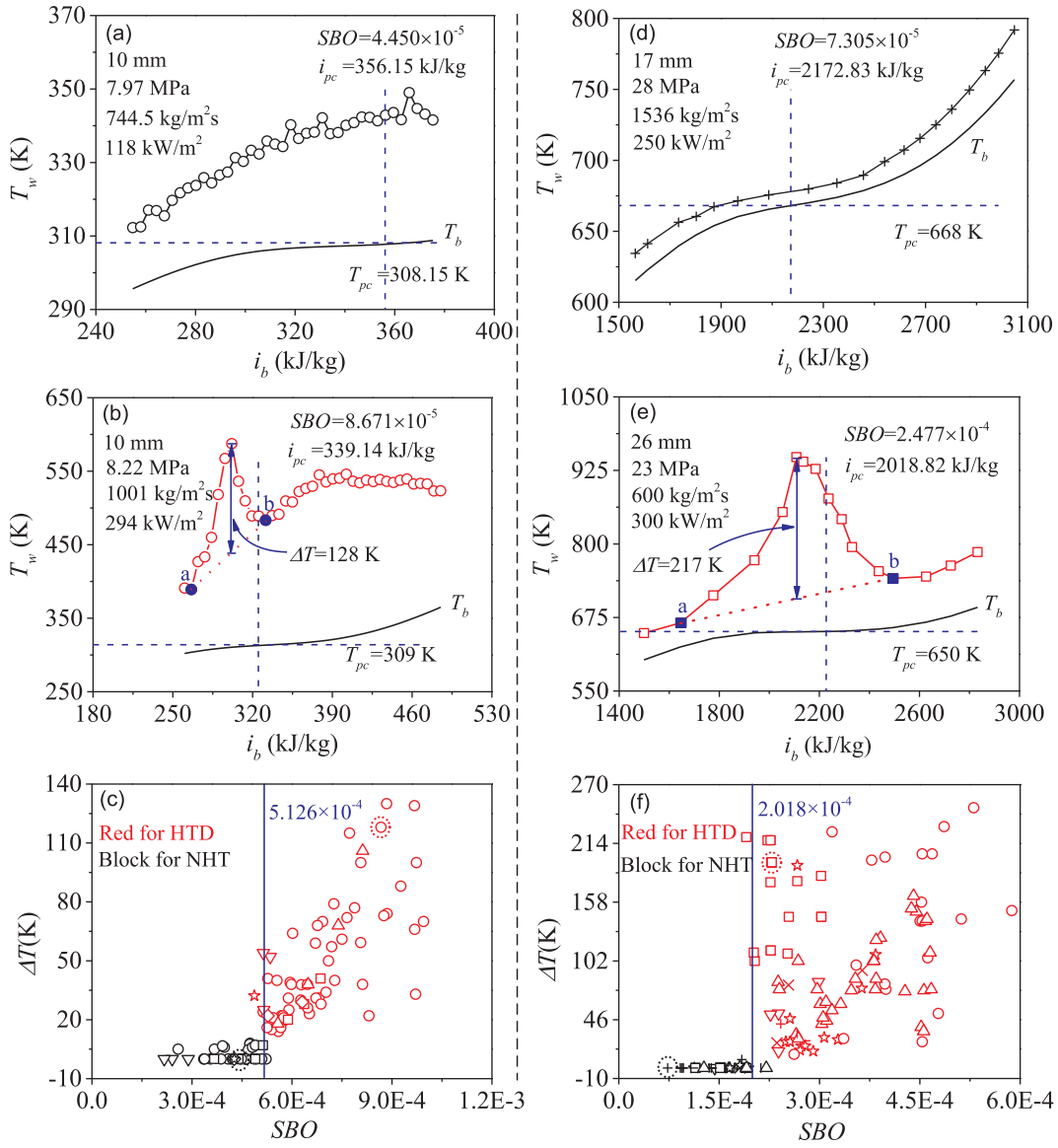

Fig. 8. The supercritical boiling number distinguishes the two regimes of heat transfer. (a)–(c) for supercritical CO_2: ○&○ for our data, ☆&☆ from Li et al (2010) with 8.80 MPa/315 kg/m^2 s/13.6–51.9 kW/m^2/2 mm; ◇&◇ from Kim and Kim (2011) with 7.532–8.194 MPa/488–492 kg/m^2 s/73.5–103.1 kW/m^2/4.5 mm; ▽&▽ from Bae et al (2010) with 7.75–8.12 MPa/285–600 kg/m^2 s/30–70 kW/m^2/6.32 mm; □&□ from Jiang (2015) with 8.35 MPa/1004–1502 kg/m^2 s/125–350 kW/m^2/8 mm; △&△ from Liu et al (2017) with 7.61 MPa/901.8 kg/m^2 s/175.9–256.2 kW/m^2/10 mm. (d)–(f) for supercritical water: △&△ from Zhao et al (2014); Li et al (2011); Wang (2012) with 23–26 MPa/459.8–1520.6 kg/m^2 s/129–1154 kW/m^2/7.6 mm; ○&○ from Zhang et al (2012); Wang et al (2013) with 23–26 MPa/450–2021 kg/m^2 s/450–1385 kW/m^2/10 mm; ▽&▽ from Hu et al. (2001) with 22.5–24 MPa/600–1000 kg/m^2 s/300–500 kW/m^2/16 mm; +&+ from Pan et al (2011); Shen et al (2014) with 22.5–30 MPa/1009–1626 kg/m^2 s/216–649 kW/m^2/17 mm; ☆&☆ from Wang et al (2011); Ackerman (1970); Shen et al (2016) with 24.8–26 MPa/406–1200 kg/m^{2}s/157–660 kW/m^2/18.5–19.8 mm; ×&× from Ackerman (1970) with 24.8 MPa/406 kg/m^2 s /157–315 kW/m^2/24.4 mm; □&□ from Lei et al (2017); Zhu et al (2009); Hu (2001) with 23–30 MPa/600–1200 kg/m^2 s/200–400 kW/m^2/26 mm; | & | from Mokry et al (2011) with 24.1 MPa/543 kg/m^2 s/252–316 kW/m^2/38 mm.

5. Conclusions

Supercritical fluid has been recognized as having single-phase structure. Correspondingly, supercritical heat transfer is treated by considering the variations of physical properties, buoyancy effect and acceleration effect. The heat transfer correlations in literature are either valid in narrow data ranges, or varied from case to case. Even though the single-phase assumption of supercritical fluids has been questioned by physicists in recent years, the pseudo-boiling concept has never been used for the theoretical treatment of supercritical heat transfer.

Here, the pseudo-boiling of supercritical heat transfer is assumed. Heat transfer is analogized between supercritical pressure and subcritical pressure, resulting in a new non-dimensional parameter of *SBO*, which reveals the competition of the momentum force due to vapor expansion against the inertia force. The S-CO_2 heat transfer experiment covered a wide range of parameters. The running pressures are up to three times of the critical pressure of CO_2. The newly obtained experimental data, together with other data sources in the literature, are used to construct a heat transfer regime map. We found that the regimes of normal heat transfer and heat transfer deterioration are interfaced at a critical *SBO*, which equals to 5.126×10^{-4} for CO_2. Sudden changes from normal heat transfer to heat transfer deterioration are also observed for supercritical fluids of water, R134a and R22. Different working fluids have different critical *SBO* to switch NHT to HTD.

We provide a solid treatment to calculate the critical heat flux for supercritical heat transfer, which is interest to various heat exchanger

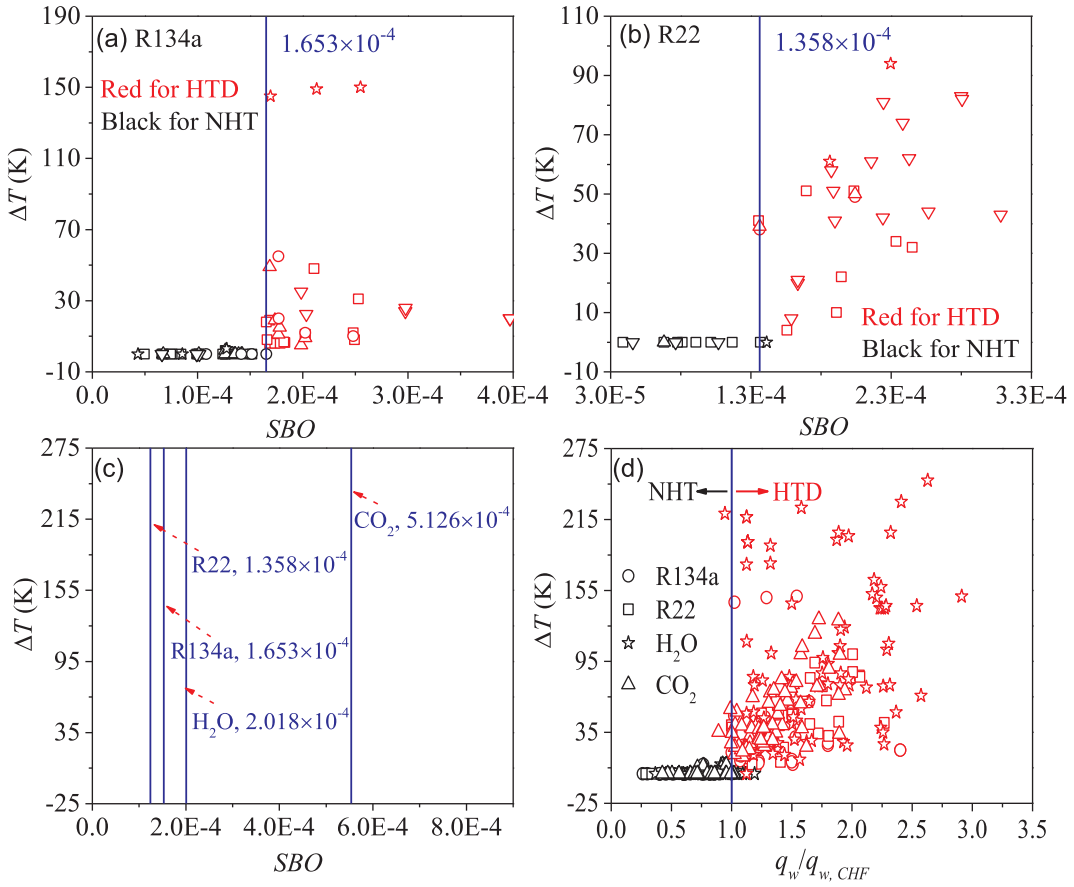

Fig. 9. Sudden changes between normal heat transfer and heat transfer deterioration across the critical supercritical boiling number *SBO* for four fluids. (a) for R134a: □&□ from Zhang (2015) with 3.9–4.7 MPa /600–2500 kg/m^2 s/20–180 kW/m^2/7.6 mm; ▽&▽ from Cui and Wang (2018a); Cui and Wang (2018b) with 4.3–4.8 MPa/500–1500 kg/m^2 s/20–80 kW/m^2/8 mm; ☆&☆ from Kang and Chang (2009) with 4.3 MPa/600 kg/m^2 s/10.21–60.09 kW/m^2/9.4 mm; △&△ from Zhang (2015) with 4.3–4.7 MPa/600–2500 kg/m^2 s/30–140 kW/m^2/10 mm; ○&○ from Chen et al. (2016) with 4.5–4.7 MPa/400–700 kg/m^2 s/30–50 kW/m^2/25 mm. (b) for R22: □&□ from Yamashita et al. (2003) with 5.5 MPa/400–1500 kg/m^2 s/10–90 kW/m^2/4.4 mm; ▽&▽ from Dubey et al. (2018) with 5.5 MPa/535 kg/m^2 s /9–60.5 kW/m^2/6 mm; ○&○ from Yamashita et al. (2003) with 5.5 MPa /400 kg/m^2 s/10–30 kW/m^2/9 mm; △&△ from Yamashita et al. (2003) with 5.5 MPa/400 kg/m^2 s/10–30 kW/m^2/13 mm; ☆&☆ from Dubey et al. (2018) with 5.5 MPa/100.7–964 kg/m^2 s/65.9–124.6 kW/m^2/13.5 mm. (d) □&□ for R22; ○&○ for R134a; ☆&☆ for H_2O; △ & △ for CO_2.

Table 1
The critical pressure and temperature for the four working fluids.

Fluid	Critical pressure (MPa)	Critical temperature (K)	Enthalpy at the critical point (kJ/kg)	Critical *SBO* from NHT to HTD
CO_2	7.38	304.1	314.44	5.126×10^{-4}
H_2O	22.06	647.1	2176.8	2.018×10^{-4}
R134a	4.06	374.2	382.10	1.653×10^{-4}
R22	4.99	369.3	373.71	1.358×10^{-4}

designs for thermal-power conversion. Future works are recommended as follows: fundamental studies of the heterogeneous structure of supercritical fluids, verification of the *SBO* effectiveness by expanding database including more working fluids, various tube inclination angles and non-uniform heating conditions, and development of heat transfer coefficients using *SBO*.

Acknowledgements

The study was supported by National Key R&D Program of China (2017YFB0601801) and National Natural Science Foundation of China (51806065).

Declaration of Competing Interest

The authors declare no competing interests.

Appendix A. Supplementary material

Supplementary data to this article can be found online at https://doi.org/10.1016/j.solener.2019.11.036.

References

Ackerman, J.W., 1970. Pseudoboiling heat transfer to supercritical pressure water in smooth and ribbed tubes. J. Heat Transfer 92, 490.
Aprea, C., Maiorino, A., 2011. An experimental investigation of the global environmental impact of the R22 retrofit with R422D. Energy 36, 1161–1170.
Bae, Y.Y., Kim, H.Y., Kang, D.J., 2010. Forced and mixed convection heat transfer to supercritical CO_2 vertically flowing in a uniformly-heated circular tube. Exp. Therm. Fluid Sci. 34, 1295–1308.
Banuti, D.T., 2015. Crossing the Widom-line–supercritical pseudo-boiling. J. Supercrit. Fluids 98, 12–16.
Berche, B., Henkel, M., Kenna, R., 2009. Critical phenomena: 150 years since Cagniard de la Tour. J. Phys. Studies 13, 3201–3209.
Bolmatov, D., Brazhkin, V.V., Trachenko, K., 2013. Thermodynamic behaviour of supercritical matter. Nat. Commun. 4, 2331.
Cengel, Y.A., Boles, M.A., 2006. Thermodynamics: An Engineering Approach, fifth ed. (McGraw-Hill Education).
Cheang, V.T., Hedderwick, R.A., McGregor, C., 2015. Benchmarking supercritical carbon dioxide cycles against steam Rankine cycles for concentrated solar power. Sol. Energy 113, 199–211.

Chen, J.Y., Xiong, Z.Q., Xiao, Y., Gu, H.Y., 2016. Experimental study on convective heat transfer of supercritical R134a in vertical circular tubes. Nucl. Pow. Eng. 37, 27–31.
Cui, Y.L., Wang, H.X., 2018a. Experimental study on convection heat transfer of R134a at supercritical pressures in a vertical tube for upward and downward flows. Appl. Therm. Eng. 129, 1414–1425.
Cui, Y.L., Wang, H.X., 2018b. In-tube convection heat transfer research of R134a under supercritical pressures. Proc. CSEE 38 (8), 2–7.
Dubey, S.K., Vedula, R.P., Iye, K.N., Gaikwad, A.J., 2018. Local heat transfer coefficient measurements using thermal camera for upward flow of Freon 22 in a vertical tube at supercritical conditions and development of correlations. Nucl. Eng. Des. 328, 80–94.
Gallo, P., Corradini, D., Rovere, M., 2014. Widom line and dynamical crossovers as routes to understand supercritical water. Nat. Commun. 5, 5806.
Gorelli, F.A., Bryk, T., Krisch, M., Ruocco, G., Santoro, M., Scopigno, T., 2013. Dynamics and thermodynamics beyond the critical point. Sci. Rep. 3, 1203.
Holman, J.P., Rea, S.N., Howard, C.E., 1965. Forced convection heat transfer to Freon 12 near the critical state in a vertical annulus. Int. J. Heat Mass Transfer 8, 1095–1100.
Hu, Z.H., 2001. Heat Transfer Characteristics of Vertical Upflow and Inclined Tubes in the Supercritical Pressure and Near-Critical Pressure Region. PhD thesis, Xian Jiaotong Universty.
Hu, Z.H., Chen, T.K., Sun, D., 2001. Experimental investigation of heat transfer characteristics of vertical smooth tubes and internally ribbed ones in near-critical and supercritical. J. Eng. Therm. Energy Pow. 16, 267–270.
Huang, D., Wu, Z., Sunden, B., Li, W., 2016. A brief review on convection heat transfer of fluids at supercritical pressures in tubes and the recent progress. Appl. Energy 162, 494–505.
Jiang, K., 2015. An Experimental Facility for Studying Heat Transfer in Supercritical Fluids. PhD thesis, Ottawa-Carleton Institute for Mechanical and Aerospace Engineering.
Kandlikar, S.G., 2004. Heat transfer mechanisms during flow boiling in microchannels. J. Heat Transfer 126, 8–16.
Kang, K.H., Chang, S.H., 2009. Experimental study on the heat transfer characteristics during the pressure transients under supercritical pressures. Int. J. Heat Mass Transfer 52, 4946–4955.
Kim, D.E., Kim, M.H., 2011. Experimental investigation of heat transfer in vertical upward and downward supercritical CO_2, flow in a circular tube. Int. J. Heat Fluid Flow 32, 176–191.
Kim, J.K., Jeon, K.H., Yoo, J.Y., Lee, J.S., 2005. Experimental Study on heat transfer characteristics of turbulent supercritical flow in vertical circular/non-circular tubes. The 11th International Topical Meeting on Nuclear Reactor Thermal-Hydraulics, October 2 − 6 (Avignon, France).
Kiran, E., Debenedetti P.G., Peters C.J., 2000. Supercritical Fluids: Fundamentals and Applications. NATO Science Series E: Applied Sciences 366 (Boston, Kluwer Academic Publishers).
Kurganov, V.A., Zeigarnik, Y.A., Maslakova, I.V., 2012. Heat transfer and hydraulic resistance of supercritical-pressure coolants. Part I: Specifics of thermophysical properties of supercritical pressure fluids and turbulent heat transfer under heating conditions in round tubes (state of the art). Int. J. Heat Mass Transfer 55, 3061–3075.
Lei, X.L., Li, H.X., Zhang, W.Q., Dinh, N.T., Guo, Y.M., Yu, S.Q., 2017. Experimental study on the difference of heat transfer characteristics between vertical and horizontal flows of supercritical pressure water. Appl. Therm. Eng. 113, 609–620.
Li, H.B., Yang, Y., Gu, H.Y., Zhao, M., Liu, D.H., 2011. Heat transfer deterioration of supercritical water in upright tube. Progr. Report China Nucl. Sci. Technol. 880–887.
Liu, S.H., Huang, Y.P., Liu, G.X., Wang, J.F., Leung, L.K.H., 2017. Improvement of buoyancy and acceleration parameters for forced and mixed convective heat transfer to supercritical fluids flowing in vertical tubes. Int. J. Heat Mass Transfer 106, 1144–1156.
Li, Z.H., Jiang, P.X., Zhao, C.R., Zhang, Y., 2010. Experimental investigation of convection heat transfer of CO_2 at supercritical pressures in a vertical circular tube. Int. J. Therm. Sci. 34, 1162–1171.
Mayinger, F., Scheldt, M., 1984. Heat transfer in the supercritical region with vertical upflow. Heat. Mass Transfer 18, 207–214.
McHardy, J., Sawan, S.P., 1998. Supercritical Fluid Cleaning: Fundamentals. Technology and Applications (Westwood, Noyes Publications).
Mokry, S., Pioro, I., Farah, A., King, K., Gupta, S., Peiman, W., Kirillov, P., 2011. Development of supercritical water heat transfer correlation for vertical bare tubes. Nucl. Eng. Des. 241, 1126–1136.
Negoescu, C.C., Li, Y., Al-Duri, B., Ding, E.L., 2017. Heat transfer behaviour of supercritical nitrogen in the large specific heat region flowing in a vertical tube. Energy 134, 1096–1106.
Pan, J., Yang, D., Dong, Z.C., Zhu, T., Bi, Q.C., 2011. Experimental investigation on heat transfer characteristics of water in vertical upward tube under supercritical pressure. Nucl. Pow. Eng. 32, 75–80.
Pizzarelli, M., 2018. The status of the research on the heat transfer deterioration in supercritical fluids: a review. Int. J. Heat Mass Transfer 95, 132–138.
Shen, Z., Yang, D., Chen, G.M., Xiao, F., 2014. Experimental investigation on heat transfer characteristics of smooth tube with downward flow. Int. J. Heat Mass Transfer 68, 669–676.
Shen, Z., Yang, D., Xie, H.Y., Nie, X., Liu, W., Wang, S., 2016. Flow and heat transfer characteristics of high-pressure water flowing in a vertical upward smooth tube at low mass flux conditions. Appl. Therm. Eng. 102, 391–401.
Shiralkar, B.S., Griffith, P., 1969. Deterioration in heat transfer to fluids at supercritical pressures and high heat fluxes. J. Heat Transfer Trans. ASME 91, 27–36.
Simeoni, G.G., Bryk, T., Gorelli, F.A., Krisch, M., Ruocco, G., Santoro, M., Scopigno, T., 2010. The Widom line as the crossover between liquid-like and gas-like behaviour in supercritical fluids. Nat. Phys. 6, 503–507.
Stein, W.H., Buck, R., 2017. Advanced power cycles for concentrated solar power. Sol. Energy 152, 91–105.
Stewart, E., Stewart, P., Watson, A., 1973. Thermo-acoustic oscillations in forced convection heat transfer to supercritical pressure water. Int. J. Heat Mass Transfer 16, 257–270.
Sun, E.H., Xu, J.L., Li, M.J., Liu, G.L., Zhu, B.G., 2018. Connected-top-bottom-cycle to cascade utilize flue gas heat for supercritical carbon dioxide coal fired power plant. Energy Convers. Manage. 172, 138–154.
Wang, F., Yang, Y., Gu, H.Y., Zhao, M., Li, H.B., Lu, D.H., 2013. Experimental research on heat transfer performance of supercritical water in vertical tube. Atomic Energy Sci. Tech. 47, 933–939.
Wang, L., 2012. Research on Heat Transfer Characteristics of Supercritical Water in the Vertical Tube. Master thesis. Shanghai Jiaotong University.
Wang, J.G., Li, H.X., Yu, S.Q., Chen, T.K., 2011. Comparison of the heat transfer characteristics of supercritical pressure water to that of subcritical pressure water in vertically-upward tubes. Int. J. Multiphase Flow 37, 769–776.
Xu, J.L., Sheng, S., Gan, Y.H., Li, Y.X., Zhang, W., Su, Q.C., 2005. Transient flow pattern based microscale boiling heat transfer mechanisms. J. Micromech. Microeng. 15, 1344–1361.
Xu, J.L., Sun, E.H., Li, M.J., Liu, H., Zhu, B.G., 2018. Key issues and solution strategies for supercritical carbon dioxide coal fired power plant. Energy 159, 227–246.
Yamashita, T., Yoshida, S., Mori, H., Morooka, S., Komita, H., 2003. Heat transfer study under supercritical pressure conditions for single rod test section. GENES4/ANP2003, 1119.
Zhang, G., Zhang, H., Gu, H.Y., Yang, Y.H., Cheng, X., 2012. Experimental and numerical investigation of turbulent convective heat transfer deterioration of supercritical water in vertical tube. Nucl. Eng. Des. 248, 226–237.
Zhang, Q., Li, H.X., Lei, X.L., Zhang, J., Kong, X.F., 2018. Study on identification method of heat transfer deterioration of supercritical fluids in vertically heated tubes. Int. J. Heat Mass Tran. 127, 674–686.
Zhang, S.Y., 2015. Experimental and Fluid Scaling Studies on the Convective Heat Transfer of Supercritical Fluid. PhD thesis, Shanghai Jiaotong University.
Zhao, M., Gu, H.Y., Cheng, X., 2014. Experimental study on heat transfer of supercritical water flowing downward in circular tubes. Ann. Nucl. Energy 63, 339–349.
Zhu, X.J., Bi, Q.C., Yang, D., Chen, T.K., 2009. An investigation on heat transfer characteristics of different pressure steam-water in vertical upward tube. Nucl. Eng. Des. 239, 381–388.